

Contents lists available at [ScienceDirect](https://www.sciencedirect.com)

Materials Science & Engineering C

journal homepage: www.elsevier.com/locate/msec

Biocompatibility evaluation of a 3D-bioprinted alginate-GelMA-bacteria nanocellulose (BNC) scaffold laden with oriented-growth RSC96 cells

Zongxi Wu^{a,b,c,d}, Shang Xie^{a,b,c,d}, Yifan Kang^{a,b,c,d}, Xiaofeng Shan^{a,b,c,d}, Qing Li^{b,c,d,e},
 *, Zhigang Cai^{a,b,c,d,**}

^a Oral and Maxillofacial Surgery, Peking University School and Hospital of Stomatology, Beijing, China

^b National Clinical Research Center for Oral Diseases, Beijing, China

^c National Engineering Laboratory for Digital and Material Technology of Stomatology, Beijing, China

^d Beijing Key Laboratory of Digital Stomatology, Beijing, China

^e Center of Digital Dentistry, Peking University School and Hospital of Stomatology, Beijing, China

ARTICLE INFO

Keywords:

3D bioprinting
 Alginate
 GelMA
 Bacterial nanocellulose
 Neural tissue engineering

ABSTRACT

Peripheral nerve injury can cause various degrees of damage to the morphological structure and physiological function of the peripheral nerve. At present, compared with “gold standard” autologous nerve transplantation, tissue engineering has certain potential for regeneration and growth; however, achieving oriented guidance is still a challenge. In this study, we used 3D bioprinting to construct a nerve scaffold of RSC96 cells wrapped in sodium alginate/gelatin methacrylate (GelMA)/bacterial nanocellulose (BNC) hydrogel. The 5% sodium alginate+5% GelMA+0.3% BNC group had the thinnest lines among all groups after printing, indicating that the inherent shape of the scaffold could be maintained after adding BNC. Physical and chemical property testing (Fourier transform infrared, rheometer, conductivity, and compression modulus) showed that the 5% alginate+5% GelMA+0.3% BNC group had better mechanical and rheological properties. Live/dead cell staining showed that no mass cell death was observed on days 1, 3, 5, and 7 after printing. In the 5% alginate+5% GelMA group, the cells grew and formed linear connections in the scaffold. This phenomenon was more obvious in the 5% alginate+5% GelMA+0.3% BNC group. In the 5% alginate+5% GelMA+0.3% BNC group, S-100 β immunofluorescence staining and cytoskeleton staining showed oriented growth. Polymerase chain reaction (PCR) array results showed that mRNA levels of related neurofactors ASCL1, POU3F3, NEUROG1, DLL1, NOTCH1 and ERBB2 in the 5%GelMA+0.3%BNC group were higher than those of other groups. Four weeks after implantation in nude mice, RSC96 cells grew and proliferated well, blood vessels grew, and S-100 β immunofluorescence was positive. These results indicate that a 3D-bioprinted sodium alginate/GelMA/BNC composite scaffold can improve cell-oriented growth, adhesion and the expression of related factors. This 3D-bioprinted composite scaffold has good biocompatibility and is expected to become a new type of scaffold material in the field of neural tissue engineering.

1. Introduction

Peripheral nerve injury includes all damage to the morphological structure or physiological function of the peripheral nerve. [1]. Clinical manifestations are mainly motor nerve, sensory nerve and autonomic nerve dysfunction and bone muscular atrophy [2]; these manifestations result in physical disability, chronic pain, loss of motor and sensory

functions, and decreased quality of life [3]. Currently, the gold standard for the clinical repair of peripheral nerve defects is autologous nerve transplantation [4]. However, it has disadvantages such as nerve torsion, dislocation, limited nerve donor area and loss of nerve function in the donor area. Therefore, nerve guide conduits (NGCs) created by tissue engineering to repair nerve defects have become the current research trend [5]. Among numerous tissue engineering methods, 3D bioprinting

* Correspondence to: Q. Li, Center of Digital Dentistry, Peking University School & Hospital of Stomatology, 22 Zhongguancun South Avenue, Haidian District, Beijing 100081, China.

** Correspondence to: Z. Cai, Department of Oral and Maxillofacial Surgery, Peking University School & Hospital of Stomatology, 22 Zhongguancun South Avenue, Haidian District, Beijing 100081, China.

E-mail addresses: qingli@hsc.pku.edu.cn (Q. Li), c2013xs@163.com (Z. Cai).

<https://doi.org/10.1016/j.msec.2021.112393>

Received 27 May 2021; Received in revised form 27 July 2021; Accepted 20 August 2021

Available online 25 August 2021

0928-4931/© 2021 Elsevier B.V. All rights reserved.

enables personalized printing and precise three-dimensional structure, thereby greatly improving the possibility of nerve defect repair [6]. Yoo et al. [7] used 3D printing to prepare an oriented collagen hydrogel using polylactide-caprolactone (PLCL) as a raw material and obtained micro-scale hydrogel patterns with a good effect on axon regeneration and remyelination. However, few studies have focused on cells containing 3D-bioprinted components, which would guide cell-directed growth in the given material strand to reduce postoperative nerve torsion or misalignment.

Sodium alginate is a linear polysaccharide that has good hydrophilicity and histocompatibility. It can be cross-linked by CaCl_2 to increase its mechanical strength [8]. In previous research [9], we used 3D bioprinting to create a gelatin-sodium alginate nerve conduit loaded with rat Schwann cells. The results show that 3D bioprinting helps cell adhesion and the expression of nerve regeneration-related genes, but the strength of the scaffold remains to be improved. Gelatin methacrylate (GelMA) is obtained by the reaction of gelatin and methacrylic anhydride. The introduction of the MA group makes it photosensitive, which has attracted wide attention in the field of nerve regeneration [10]. Studies have confirmed that Schwann cells can attach and proliferate on GelMA and GelMA-pHEMA (5:5) hydrogels [11], whereas Zhu et al. [12] used GelMA and poly (ethylene glycol) diacrylate (PEGDA) to print NGCs with microchannels and found that the nerve fibres could enter the microchannel through the branch and extend to the distal end of the injury site. Therefore, combining sodium alginate-GelMA as the main component of the nerve conduit scaffold can provide an important microenvironment and microchannel structure for the regeneration of peripheral nerves.

Interpenetrating network (IPN) polymer hydrogels are a special type of hydrogel formed by IPNs containing hydrophilic groups after absorbing water [13]. Calcium alginate-GelMA can be used as an IPN hydrogel, and the application of nanomaterials can further improve the mechanical strength of the IPN. Bacterial nanocellulose (BNC) is composed of interconnected cellulose ribbons. Due to its good biocompatibility and mechanical properties, it has been suggested to be an effective hydrogel-like material [14]. Sämfors et al. [15] used BNC to construct a blood vessel scaffold, in which human umbilical vein endothelial cells were inoculated and cultured to form a unidirectional arrangement after 7 days. Adding BNC to the calcium alginate-GelMA double network system to form a semi-network rigid structure is expected to further enhance the mechanical strength of the scaffold.

In previous studies, researchers used nanocellulose and GelMA hybrids to print scaffolds, which helped maintain the activity of ATDC5 cells within 7 days [16]. There are also studies that used sodium alginate and GelMA for hybrid printing [17]. To enhance mechanical properties and promote cell-oriented growth, 3D bioprinting of sodium alginate, GelMA and BNC was used in the field of peripheral nerve regeneration. Therefore, in conjunction with the findings of our previous studies, we explored the printability of alginate, GelMA and BNC hybrid bioink at different concentrations and examined the physicochemical properties of the material. Then, the bioink was mixed with RSC96 cells for bioprinting. Cell viability analysis, cell proliferation, immunofluorescence staining, cytoskeleton staining and a PCR array were performed to verify the effects of different concentrations of bioink on RSC96 cells. Finally, its biocompatibility was verified subcutaneously in nude mice.

2. Material and methods

2.1. Materials ratio experiment

The sodium alginate used in this study was purchased from Sigma Aldrich (180947), GelMA was purchased from Aladdin (Lot# F1821011), BNC was purchased from Qihong Technology (Qihong Technology), and lithium phenyl(2,4,6-trimethylbenzoyl) phosphinate (LAP) was purchased from TCI Shanghai (L0290). Co60 was used to irradiate GelMA and sodium alginate before configuring the bioink.

High temperature and high pressure were used to sterilize BNC. As shown in Fig. 2a, different concentrations of sodium alginate were dissolved with GelMA in phosphate-buffered saline (PBS) solution, and the proportion of materials capable of extrusion fluency was selected according to Fig. 2b-d. Finally, 5% was selected as the final concentration of sodium alginate, in which 0.5% LAP was added as the photoinitiator, and the final experiments were grouped as follows: ① 5% sodium alginate+0.5% LAP+2.5% GelMA, ② 5% sodium alginate+0.5% LAP+5% GelMA, ③ 5% sodium alginate+0.5% LAP+10%GelMA, and ④ 5% sodium alginate+0.5% LAP+5% GelMA+0.3% BNC. (The following abbreviations are: ①2.5% GelMA; ②5% GelMA; ③10% GelMA; and ④5% GelMA+0.3%BNC). Image J was used to measure the filament diameter of different groups, and the average value($n = 5$) was taken for statistical analysis.

2.2. Materials physicochemical properties

2.2.1. Modulus-temperature analysis, viscosity-shear rate analysis and viscosity-temperature analysis

To evaluate the rheological properties of the bioink in each group, a rotational rheometer (Discovery HR2; TA Instruments, Inc., USA) was used to test the storage modulus (G'), loss modulus (G'') and composite viscosity of the bioink in each group. To evaluate the relationship between the storage modulus (G'), loss modulus (G'') and temperature, each bioink was scanned for 750 s at a frequency of 1 Hz, at 1% strain and over a range of 9.95 °C–37.08 °C to obtain modulus-temperature curves. To determine the relationship between the composite viscosity and shear rate of bioink in each group, the bioink was scanned for a time period of 200 s at 1% strain and 20 °C temperature and 0.1–1000 shear rate to obtain the composite viscosity-shear rate curve. To further evaluate the relationship between the bioink composite viscosity and temperature, the bioink was scanned at a frequency of 1 Hz, strain of 1%, and temperature of 9.95 °C–37.08 °C for 12.5 min to obtain the composite viscosity-temperature curve. All values are shown as the mean \pm SD of three samples.

2.2.2. Thixotropic tests

In order to evaluate the thixotropic behaviour of bioinks in each group, a rotational rheometer (Discovery HR2; TA Instruments, Inc., USA). A three-step experiment was carried out at 20 °C and 1 Hz frequency. First, the state of the hydrogel before 3d bioprinting was simulated by using the shear rate of 0.1 s^{-1} for 60s, and then the shear rate was adjusted to 100 s^{-1} and maintain 10s to simulate the 3d bioprinting process. Finally, the shear rate was restored to 0.1 s^{-1} for 60s to simulate scaffold after 3d bioprinting, and the viscosity time curve was obtained and analysed.

2.2.3. Scanning electron microscopy (SEM) of the scaffold

The bioink of each group were freeze-dried, and then SEM (SU8020, Hitachi) was used to observe the micromorphology of each group of hydrogels after coating with gold. Image J was used to measure the porosity of different groups, and the average value was taken for statistical analysis.

2.2.4. Fourier infrared analysis

The chemical composition of each bioink was investigated by a NICOLET IS10 FTIR spectrometer (Thermo Fisher Scientific Inc., USA). Each sample was ground together with 200 mg KBr in an agate mortar at a ratio of approximately 1:20 and pressed into a thin slice. The flakes were placed in a sample chamber with automatic identification, the spectral range was set from 4000 to 400 cm^{-1} , the resolution was 4 cm^{-1} , and the scan time was approximately 100 s. After background and baseline corrections, FTIR spectra were analysed.

2.2.5. Analysis of electrical conductivity

The bioink from each group was lyophilized and pressed into thin sections ($n = 3$), and electrical conductivity measurements of the thin

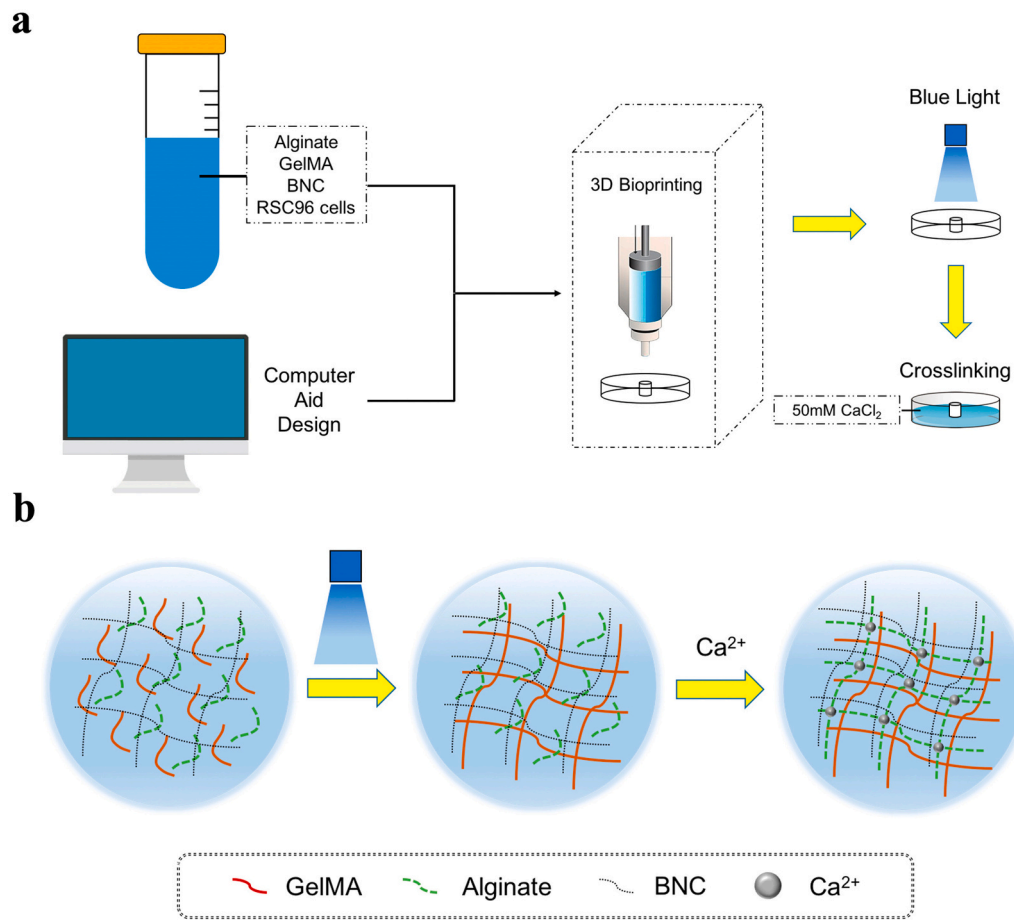


Fig. 1. a) Schematic illustration of 3D-bioprinting bioink production. b) Schematic illustration of material cross-linking at the molecular level.

sections were performed by a high-precision electrical resistivity tester (YAOS, FM100GH) using the four-probe method, with 3 averages measured at different locations of the selected samples in the measurements.

2.2.6. Compressive modulus analysis

The compressive properties of the bioinks in each group were tested using a universal testing machine. Briefly, the cross-linked hydrogels of each group were placed between load-bearing sensors with circular metal plates on a universal testing machine at room temperature, the samples were compressed to 80% deformation of their thickness at a speed of 0.5 mm/min, the data were recorded, and the compressive modulus was calculated from the slope of the stress-strain curve (linear strain range of 0–10%).

2.3. Cell culture and 3D bioprinting

RSC96 cells were purchased from ATCC and maintained in Dulbecco's modified Eagle's medium (Gibco, Grand Island, 8120185) supplemented with 10% foetal bovine serum (Gibco, 10099–141) and 1% penicillin/streptomycin (Gibco, 15140–122). Cells were cultured in the humidified environment of a 37 °C incubator and passaged every 2 days. Cells from passages 9–13 were used for experiments. The process of 3D bioprinting is shown in Fig. 1a. Briefly, a cuboid with a length of 8 mm, width of 8 mm and height of 2 mm and a cylinder 5 mm in height and 4 mm in diameter were designed using computer design software. The cuboids were then cut into 5 layers and 17 layers, respectively (S. Fig. 1). Thereafter, a 1 ml syringe was placed after mixing the cells with the bioink and placed in the Medprin bioprinter (BMP-C300-T300-IN3). In consideration of the biomimetic structure as well as printer accuracy, a

Table 1
3D-bioprinting parameters.

Parameter	Value
Barrel temperature (°C)	20–25
Ambient temperature (°C)	20
Fill density (%)	40
XY plotting speed(mm/s)	30
Inner diameter of needle(μm)	160
Layer thickness (μm)	300

printing needle with an inner diameter of 160 μm was selected. The 3D-bioprinted parameters are shown in Table 1. When the construct was printed out, it was solidified by using blue light at a wavelength of 430 nm for 20 s and cross-linked by using sterilized CaCl₂ solution at a concentration of 50 mm for 5 min (Fig. 1b). Subsequently, the construct was placed into the culture medium.

2.4. Shape fidelity

Shape fidelity is evaluated by extruding filaments from qualitative macro images and calculating printability index (Pr) [18]. The macro images of each group were processed by ImageJ software, and the perimeter and area of interconnection channel were measured ($n > 20$). Then calculate Pr value and find the pore perimeter normalized by pore area. The formula is as follows:

$$Pr = L^2/16A \quad (1)$$

where L is the perimeter and A is the area. Under ideal gelation condi-

tions or ideal printing suitability, the affirmative channel of the structure is square and the Pr value is 1. Pr = 1 means that the extrusion line has good uniformity, Pr > 1.1 means unacceptable uniformity [19].

2.5. Cell viability analysis

Cell viability in the 3D-bioprinted scaffolds was assessed using a fluorescence live/dead viability assay kit (KeyGEN Bio TECH, KGAF001, China). Briefly, 8 μ m propidium iodide (PI) and 2 μ m calcein AM were dissolved in 10 ml PBS to configure the staining solution. After incubation for 30 min with the staining solution, the scaffolds were washed 3 times with PBS buffer and observed under a fluorescence microscope (calcein AM stained viable cells green at a wavelength of 490 nm whereas PI stained dead cells red at a wavelength of 535 nm).

2.6. Cell proliferation assay

Cell Counting Kit-8 (CCK8, LK815, Japan) was used to evaluate cell proliferation of the 3D-bioprinted scaffolds on days 1, 3, 5 and 7. Briefly, CCK8 solution was mixed with culture medium at a ratio of 1:9 to obtain a working solution, and samples ($n = 3$) at each time point were incubated with 1 ml working solution for 1 h. A total of 110 μ l of the supernatant was transferred to a 96-well plate, and the absorbance (OD) value of the plate at a wavelength of 450 nm was measured using a microplate reader (BioTek ELX800, VT, USA).

2.7. S-100 β immunofluorescence staining

The 3D-bioprinted hydrogel scaffolds were subjected to S-100 β immunostaining to determine the expression of RSC96 cell signature proteins. Briefly, on day 4 after 3D bioprinting, scaffolds in each group were cross-linked with 50 mM CaCl₂ solution for another 5 min and fixed with 4% paraformaldehyde for 30 min. Scaffolds were then blocked with blocking solution (1% PBS/5% BSA/0.3% Triton X-100) for 30 min. Rabbit anti-rat S100 β antibody (Abcam, ab52642) was diluted (1:100) in antibody dilution buffer (1% PBS/1% BSA/0.3% Triton X-100). After that, scaffolds were immersed in rabbit anti-rat S100 β antibody solution overnight at 4 °C. On the next day, the residual liquid was aspirated, and scaffolds were gently rinsed 3 times with PBS. Goat anti-rabbit secondary antibody (Abcam, ab150077) was diluted to 1:500 with secondary antibody dilution buffer (1% PBS/1% BSA/0.3% Triton X-100). Samples were incubated with secondary antibody solution for 1 h. After rinsing 3 times with PBS, samples were stained with DAPI staining solution (ZSGB-BIO, ZLI-9557) for 10 min and observed under a laser confocal microscope (LMS710, Zeiss, Germany).

2.8. Cytoskeleton staining

3D-bioprinted scaffolds were stained by using 1 \times Phalloidin-iFluor 594 to observe the topography of their cytoskeletons in the scaffold. Briefly, on days 4 and 7 after printing, scaffolds were re-cross-linked using 50 mM CaCl₂ for 5 min. Then, the scaffolds were fixed with 4% paraformaldehyde for 10 min after rinsing 3 times with PBS. After 2–3 washes with PBS, the scaffold was incubated with 0.1% Triton X-100 for 3–5 min. Then, the scaffolds were stained for 30 min at room temperature by adding 1 \times phalloidin conjugate working solution (1 ml PBS + 1% BSA in 1 μ l 1000 \times phalloidin conjugate storage solution) after washing 2–3 times with PBS; next, DAPI staining solution was added, and the cells were observed at excitation/emission (EX/EM) = 590/618 nm using a laser confocal microscope (LMS710, Zeiss, Germany). Image J was used to calculate the angle between the long axis of the cell and vertical line of the long axis of the scaffold, and the percentage of each angle range was counted.

2.9. Quantitative real-time PCR (qRT-PCR) and PCR array analysis

QRT-PCR was used to analyse the gene expression of cells cultured for 7 days on 3D-bioprinted scaffolds of each group ($n = 3$). Scaffolds were soaked in 100 mM sodium citrate for 5 min, and hydrogels were de-cross-linked with gentle stirring. The decapsulated cells were centrifuged at 1000 rpm for 5 min after cross-linking, and the pellet was washed with PBS and centrifuged again at 1000 rpm for 3 min. Total RNA was extracted using TRIzol reagent (Invitrogen, USA) according to previous experience [20]. The PrimeScript™ RT reagent kit (Takara, Japan) was used for reverse transcription. Faststart universal SYBR Green Master Mix (Rox) (Roche, Germany, 04913850001) was used for quantitative real-time PCR. Ninety-two mRNA constructs encoding neuroregeneration-related genes were detected using a rat neurogenesis PCR array (Wcgen Biotech, Shanghai, China) according to the manufacturer's protocol ($n = 3$). Gene expression profiles were analysed according to the manufacturer's protocol (Wcgen Biotech, Shanghai, China), and data were analysed using software from Wcgen Biotech. Genes with fold change greater or less than 2.0 were considered biologically significant.

2.10. In vivo experiment, HE staining and S-100 β immunofluorescence staining

To verify the biocompatibility of 3D-bioprinted constructs containing cells in vivo, the 3D-bioprinted constructs were placed subcutaneously in nude mice for in vivo experiments. Animal experiments were carried out according to the ethical principles of the Animal Protection and Use Committee of Peking University (licence No. LA2018216). Implants were divided into two groups: the 5% GelMA group (containing RSC96 cells) and the 5% GelMA+0.3% BNC group (containing RSC96 cells). On day 1 after printing, male BALB/C nude mice (Charles River, weight 20 \pm 1 g) aged 7 weeks were randomly divided into two groups and anaesthetized with 2% chloral hydrate. Sterile implants were placed in the subcutaneous area of the back of the animal and marked accordingly ($n = 18$). All animals were kept at 20–25 °C in a 12-h light/dark cycle. At 2 and 4 weeks after the operation, the nude mice were killed by cervical dislocation, and the implants were collected. The implants were fixed with 4% formalin, dehydrated and embedded in paraffin. Slices were created using a rotary microtome with a thickness of 4–6 μ m. HE staining was performed as follows: before staining, paraffin in the section was removed with xylene and then immersed in distilled water with high to low concentrations of alcohol. Then, the slices were soaked in haematoxylin dye solution for 5–15 min, washed with tap water, differentiated with hydrochloric acid ethanol, and then washed with running water. The slice was further immersed in eosin for 3–5 min, dehydrated with pure alcohol, cleared with xylene, and finally sealed with neutral glue. The expression of S-100 β in RSC96 cells was evaluated by immunohistochemistry (IHC).

2.11. Statistical analysis

The data are expressed as the mean \pm standard deviation and were analysed by SPSS 20.0 software. In terms of statistical comparison, a *t*-test was used in this study. After confirming the homogeneity of variance, one-way ANOVA and least significant difference (LSD) tests were performed. The significance level was $\alpha = 0.05$. * $P < 0.05$ was considered statistically significant.

3. Result

3.1. Printability analysis of materials

Barros et al. [21] used a mixture of 2% sodium alginate and 7.5% GelMA to better simulate bioprinted endothelial cells to optimize the viability of endothelial cells. Zhou et al. [22] used 10% (*w/v*) GelMA, 1%

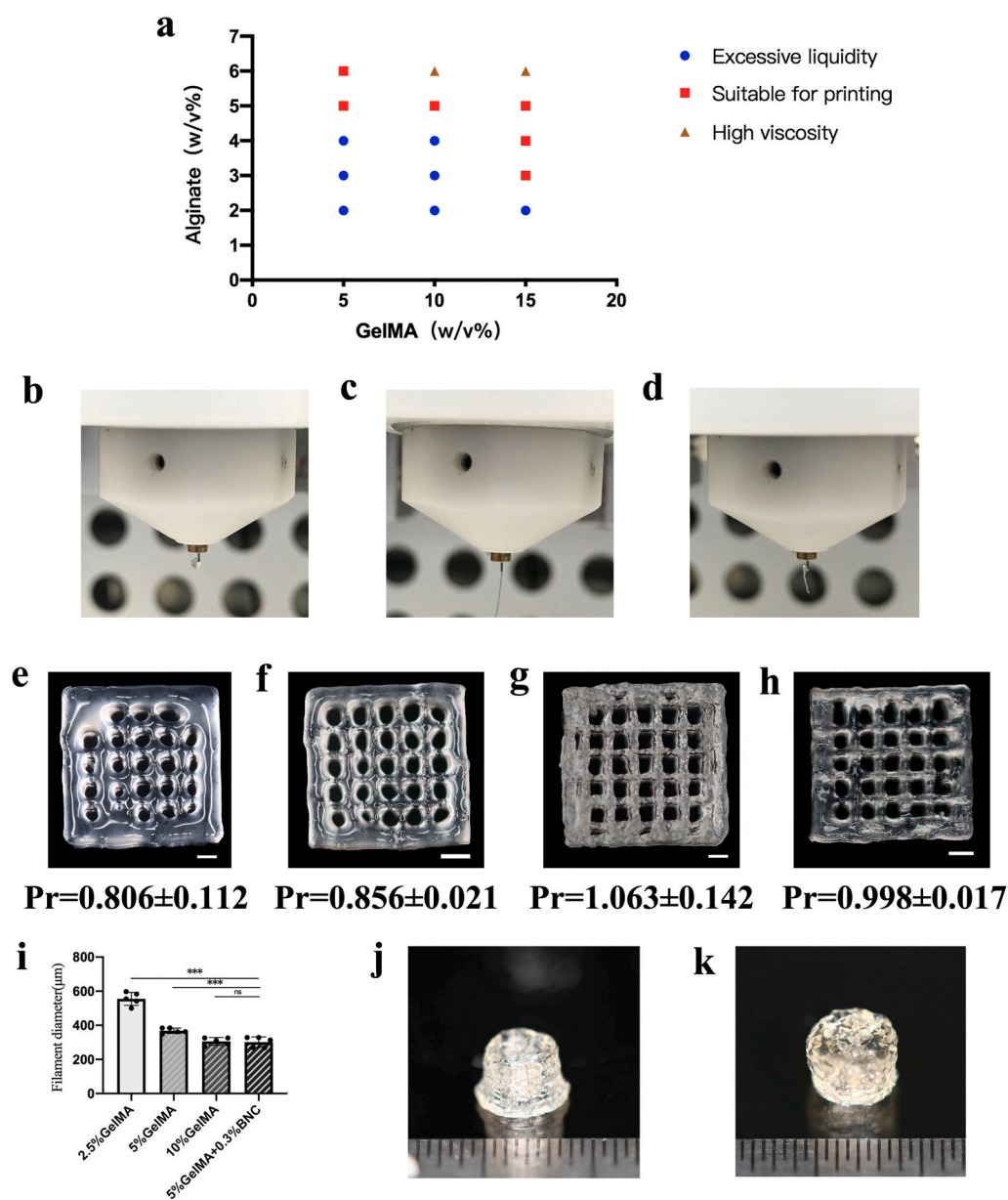


Fig. 2. Material printability: a) different concentrations of sodium alginate and GelMA, b) excessive fluidity of extruded liquid, c) extruded lines suitable for printing, d) high viscosity of extrusion lines, e) printing model of the 2.5% GelMA group (scale bar = 1 mm), f) printing model of the 5% GelMA group (scale bar = 1 mm), g) printing model of the 10% GelMA group (scale bar = 1 mm), h) printing model of the 5% GelMA+0.3% BNC group (scale bar = 1 mm), i) filament diameter of each group, j) printing cylinder model of the 5% GelMA group (scale bar = 0.5 mm), and k) printing cylinder model of the 5% GelMA+0.3% BNC group (scale bar = 0.5 mm).

(v/v) PEGDA750 and 1% (w/v) alginate as bioinks to bioprint small vessels. Our study found that the printability was mainly determined by the concentration of sodium alginate under the same temperature. When the sodium alginate concentration was 5%, different concentrations of GelMA (2.5%–15%) could be used to squeeze out the continuous lines shown in Fig. 2a, and when the concentration of sodium alginate was higher or lower, it would lead to discontinuous lines (Fig. 2d) or the mixture becoming too thin to squeeze as a liquid (Fig. 2b). Therefore, we chose a concentration of 5% sodium alginate mixed with different concentrations of GelMA as the experimental groups. Fig. 2e–i shows that after photo-cross-linking and chemical cross-linking, the 5% GelMA+0.3%BNC group ($301.49 \pm 30.59 \mu\text{m}$) and 10% GelMA group ($305.80 \pm 22.57 \mu\text{m}$) had the thinnest line among all groups, which indicated that the inherent shape of the scaffold could be maintained by adding BNCs. The next group was the 5% GelMA group ($368.12 \pm 15.71 \mu\text{m}$) and 2.5% GelMA group ($555.56 \pm 38.03 \mu\text{m}$), which showed that the higher the concentration of GelMA, the better the printability to maintain the original thickness of the line after printing without local collapse. Printability index (Pr) of each constructs were found in the

range of 0.8–1.1, and the 5%GelMA+0.3%BNC group was closer to 1, demonstrating good shape fidelity. Fonseca et al. [23] used BNC as a support for hyaluronic acid (HA) microneedles and obtained good mechanical properties. Bao et al. [24] found that when the amount of BNC increased, the mechanical strength of D-BNC and G-BNC catheters was stronger than that of many tissue-engineered blood vessels (0.4–2.2 N). According to the computer software, we designed and printed a cylinder with a diameter of 4 mm and a height of 5 mm and used it in the subsequent in vivo experiments. The height of the scaffold was higher after adding BNC (Fig. 2j–k), and the deformation of the material was smaller. Therefore, the results of this experiment confirmed that BNC could be the mechanical reinforcer and rheology modifier to the bioink.

3.2. Analysis of physical and chemical properties of materials

All samples show the same properties under stress scanning. In Fig. 3a, we found that before photocuring, the storage modulus of hydrogel in each group was basically higher than that in the loss modulus, and the storage modulus of the 10% GelMA group was higher

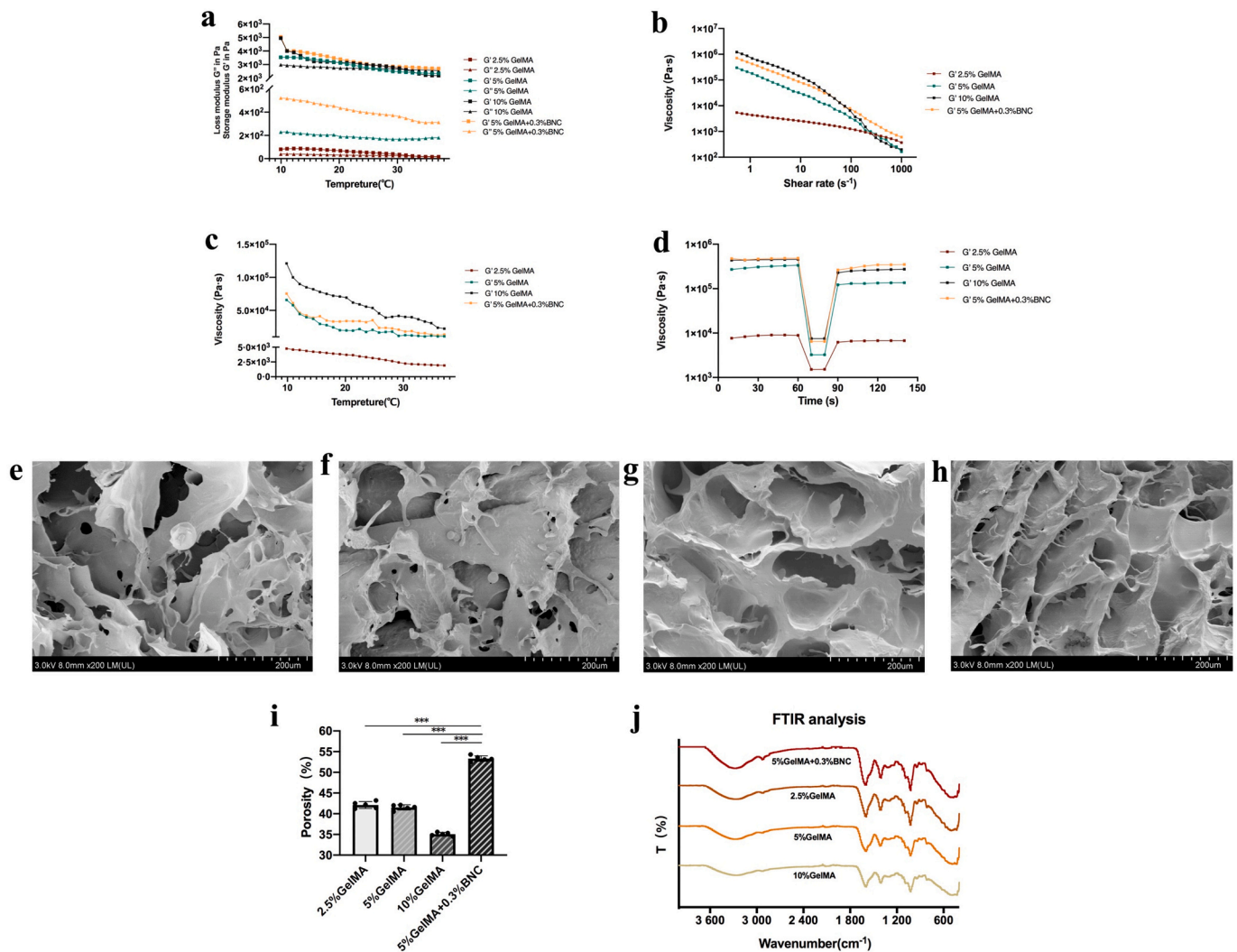


Fig. 3. Physical and chemical properties analysis of materials: a) modulus-temperature curve, b) viscosity-shear rate curve, c) viscosity-temperature curve, d) viscosity-time curve, e) SEM of the 2.5% GelMA group, f) SEM of the 5% GelMA group, g) SEM of the 10% GelMA group, h) SEM of the 5% GelMA+0.3% BNC group, i) porosity of each group, j) FTIR.

than other groups. The storage modulus of the 5% GelMA group and the 5% GelMA+0.3% BNC group were close, and the storage modulus of the 2.5% GelMA group was lowest. The relationship between viscosity and shear thinning characteristics and temperature is helpful to understand the ability of hydrogels to be extruded through 3D bioprinting to form fine structures. The shear thinning feature enables the printing nozzle to pass smoothly with reduced shear viscosity to avoid the drag of the previous printing layer, which may distort the entire printing structure [25]. Temperature is the decisive factor for the application of hydrogels in 3D bioprinting. We found that in Fig. 3b, the viscosity of each hydrogel decreased with increasing shear rate. Similarly, the viscosity of each group decreased with increasing temperature, and the 10% GelMA group had the largest reduction at 10–15 degrees, whereas the viscosity of the 2.5% GelMA group was the lowest at different temperatures. Combined with actual printing, after photocuring, the linear plasticity of the 10% GelMA group and the 5% GelMA+0.3% BNC group was better than that of the 5% GelMA group and the 2.5% GelMA group (Fig. 3c), indicating that the rheology of the hydrogel was determined by the storage modulus and viscosity. Thixotropic tests of each group (Fig. 3d) showed that when the shear rate was maintained at 0.1 s^{-1} at the appropriate temperature of $20 \text{ }^{\circ}\text{C}$, the viscosity of 5% GelMA+0.3% BNC group and 10% GelMA group was close to that of $4 \times 10^6 \text{ Pa}\cdot\text{s}$, followed by 5% GelMA group and 2.5% GelMA group, respectively.

When the shear rate increased to 100 s^{-1} , the viscosity of each group decreased significantly. When restored to 0.1 s^{-1} , the hydrogels in each group basically recovered to the first stage of viscosity, indicating that each group of hydrogels were highly thixotropic materials, which is very important for extrusion-based 3D bioprinting.

In the SEM images (Fig. 3e–h), each group of hydrogels had a porous structure, and the pores were interconnected. The porosity of the 5% GelMA+0.3% BNC group was 53.34%, higher than the 2.5% GelMA group (42.1%), 5% GelMA group (41.52%) and the 10% GelMA group (35.06%). The pore size of the 5% GelMA+0.3% BNC group was smaller and more uniform because the average pore size of the composite hydrogel could be adjusted by the BNC particle content [26].

The FTIR spectra of hydrogels in each group are shown in Fig. 3j. The results show a sodium alginate hydroxyl bond (O–H) at 3394 cm^{-1} , which may overlap with the peak at 3289 cm^{-1} (mainly N–H stretching of BNC) [27]. The strong peak at 1653 cm^{-1} is related to the tensile vibration of GelMA C=O, and the peak at 1535 cm^{-1} is related to the tensile vibration of GelMA C–N and N–H bending [28]. The peak at 1158 cm^{-1} is characteristic of BNC glycosidic bonds [29]. An overlap of the symmetrical -COO stretching (COOH group) of sodium alginate and the bending of CH in BNC may be evident at 1410 cm^{-1} . The peak at 895 cm^{-1} reflects the bending deformation of CH_2 in BNC [30]. Combined with the above results, it can be seen that the inherent characteristics of

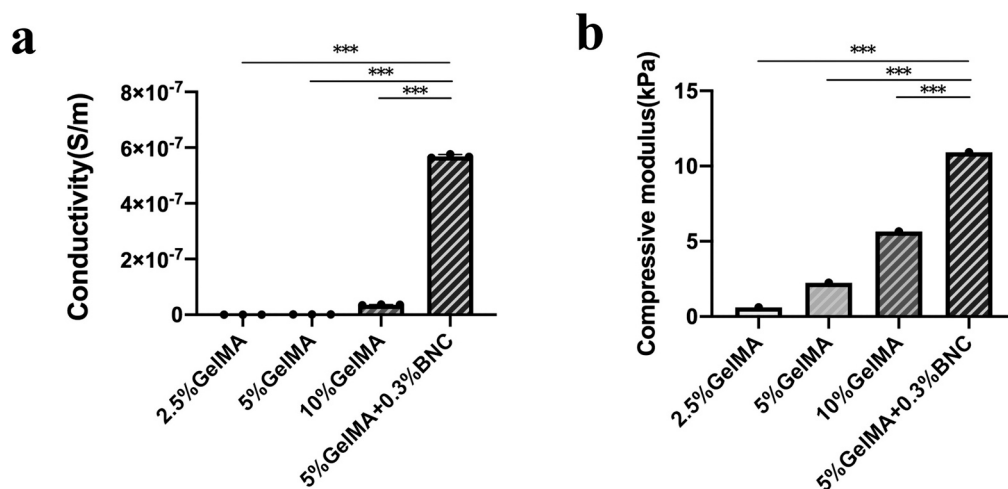


Fig. 4. a) Electrical conductivity, b) compressive modulus.

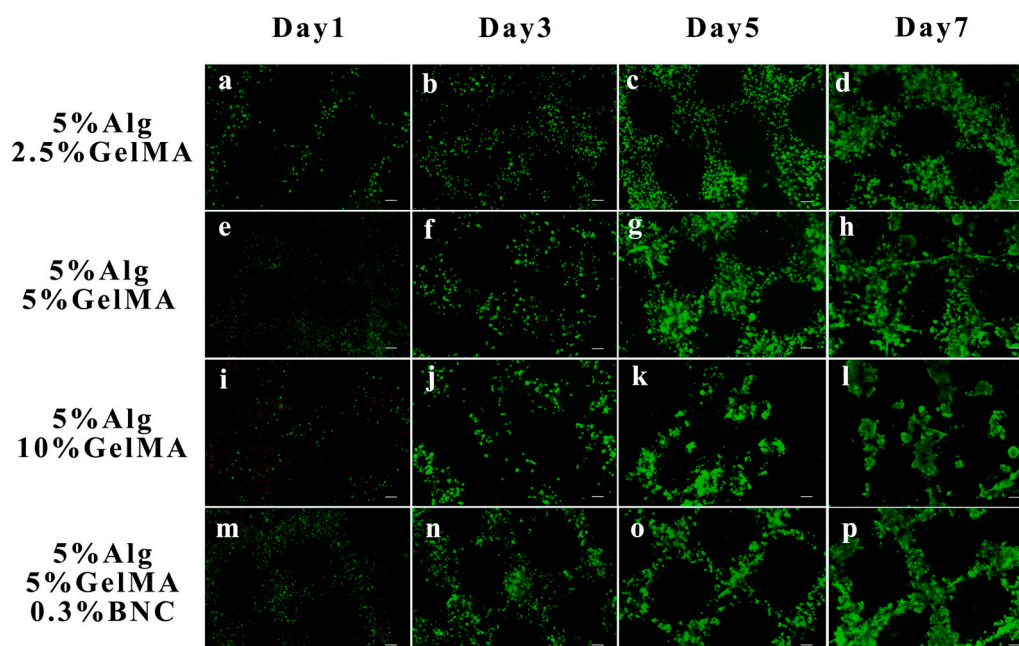


Fig. 5. Live/dead cell staining: merged images of different groups on day 1 (a, e, i, and m), day 3 (b, f, j, and n), day 5 (c, g, k, and o) and day 7 (d, h, l, and p) after 3D bioprinting. (Scale bar: 200 μ m).

sodium alginate, GelMA and BNC will not be changed in the process of 3D bioprinting.

Fig. 4a shows that the conductivity of the material is obviously enhanced after adding BNC, which is due to the porous nanostructure and abundant hydroxyl functional groups that make the active catalytic layer of BNC bind closely with the substrate [31]. Dutta et al. [32] improved the electrochemical properties of the composite by using its unique properties and network structure. The conductive substrate was prepared by in situ polymerization of polypyrrole (PPy) on BNC fibres, which has good flexibility, mechanical properties and electrical conductivity [33]. Good electrical conductivity is of great significance to nerve regeneration [34], so the addition of BNC can make the nerve conduit have a certain level of electrical conductivity.

The compression modulus of the hydrogel increased with increasing GelMA concentration when the alginate concentration was the same (Fig. 4b). The compression modulus of the 2.5% GelMA group was 0.60547 kPa, that of the 5% GelMA group was 2.24957 kPa, and that of

the 10% GelMA group was 5.65764 kPa. This is because the higher the concentration of GelMA was, the more C=C was involved in photo-cross-linking. The cross-linking between the macromolecules of GelMA was much closer, and the compression modulus of the material was higher [35]. After adding 0.3% BNC, the compression modulus of the hydrogel increased to 10.9193 kPa. This was due to the smaller diameter of BNC, which has a higher surface area than cellulose obtained from plants, and special mechanical properties. Also, its stress-strain behaviour is similar to that of soft tissue [36]. Therefore, BNC is widely used as a reinforcing material for polymer networks to maintain the shape and profile of scaffolds while ensuring biocompatibility [37–38].

3.3. Analysis of cell viability and proliferation

The viability of RSC96 cells in the 3D-bioprinted scaffold within 7 days of culture was analysed by live/dead cell staining (Fig. 5). Most of the cells in all groups were stained green, indicating that the cells had

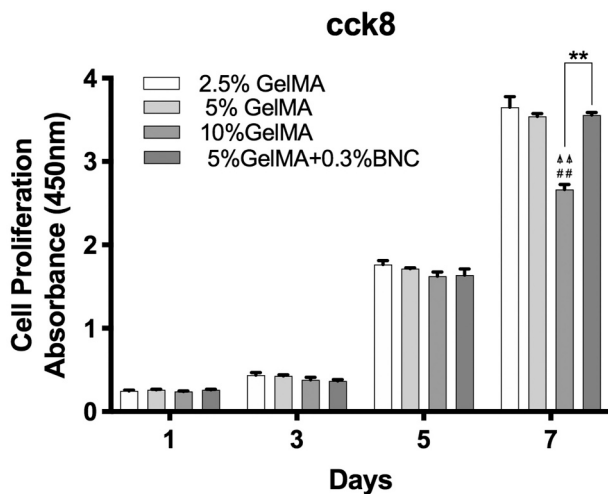


Fig. 6. Proliferation of RSC96 cells in different groups tested by CCK8. (**, #, ##, $\Delta\Delta p < 0.01$).

good vitality. From the fluorescence images taken on day 1, it could be seen that the dead cells were evenly distributed in the scaffold; no mass cell death was observed (Fig. 5a, e, i, and m). From day 1 to day 7, the number of fluorescent cells increased in all groups. Pepelanova et al. [39] proved that low concentrations of GelMA and low doses of ultraviolet (UV) light provide a proper microenvironment for mesenchymal stem cells (MSCs) to promote cell growth. MSCs are highly active in hydrogels with low gel concentrations and low UV doses. GelMA could also be used to load C2C12 cells. The cells in GelMA fibres were exposed to electrical stimulation. The results showed that relatively high cell arrangement and reasonable cell viability could be obtained at medium cell density (15×10^6 cells/mL) [40]. Combined with the results of this study, GelMA has certain biocompatibility and can promote the growth of RSC96 cells loaded with GelMA. On day 7, the 10% GelMA group (Fig. 5l) exhibited a local proliferation trend and did not grow well.

When the concentration of GelMA is high, the proliferation and growth of cells is inhibited [41]. Low-concentration GelMA ($\leq 5\%$) bioink is more attractive because its relatively loose polymer network can promote the interaction, migration and more effective metabolism between cells [42]. This outcome is similar to the results of this study, so using the appropriate concentration of GelMA is of great significance for the growth of RSC96 cells.

In addition, on day 7, the cells in the 5% GelMA group formed linear junctions and grew in the scaffold (Fig. 5h), which was more obvious in the 5% GelMA+0.3% BNC group (Fig. 5p). Pillai et al. [43] cultured human skin fibroblasts and mouse osteoblasts on a bacterial cell-based sustainable Kombucha (KBC) sheet; the results showed that they had good attachment, growth and proliferation. BNC modified by calcium phosphate and other bone minerals [44] or chitosan, gelatin and BNC hydrogels [45] can improve cell adhesion and cell proliferation. This phenomenon can be explained by durotaxis, a mechanism of cell migration. Therefore, cell migration is affected by mechanical properties (duro/mechanotaxis) [46]. Studies have shown that fibroblasts can migrate along the 3D-printed alginate, cellulose nanocrystal (CNC) and GelMA hydrogel interface [47]. This can be understood as the basic process of 3D printing and the guiding role of BNC itself to promote the orientation growth of RSC96 cells. Therefore, the results of this study confirm the effect of BNC on improving the cell adhesion property of sodium alginate-GelMA hydrogel. Moreover, compared with the other three groups, the 5% GelMA+0.3% BNC group maintained better line width on the 7th day, which further proves that BNC can not only promote cell adhesion but also increases the plasticity and mechanical strength of the bioink. In the cell proliferation experiment (Fig. 6), we found that the addition of 0.3% BNC did not significantly affect the proliferation of RSC96 cells in the scaffold, which is similar to many research results [48–49]. In contrast, when the concentration of GelMA was 10%, compared with other groups, the proliferation of RSC96 cells was affected on day 7. This result is consistent with live/dead cell staining results.

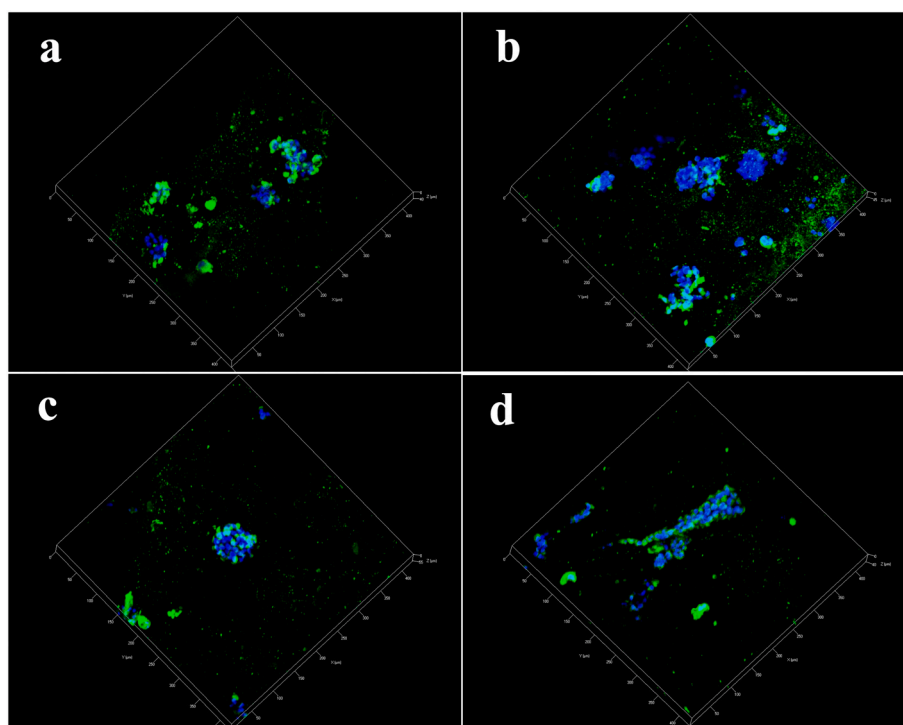


Fig. 7. Immunostaining for the S100 β marker on day 4 of a) the 2.5% GelMA group, b) 5% GelMA group, c) 10% GelMA group, d) and 5% GelMA+0.3% BNC group.

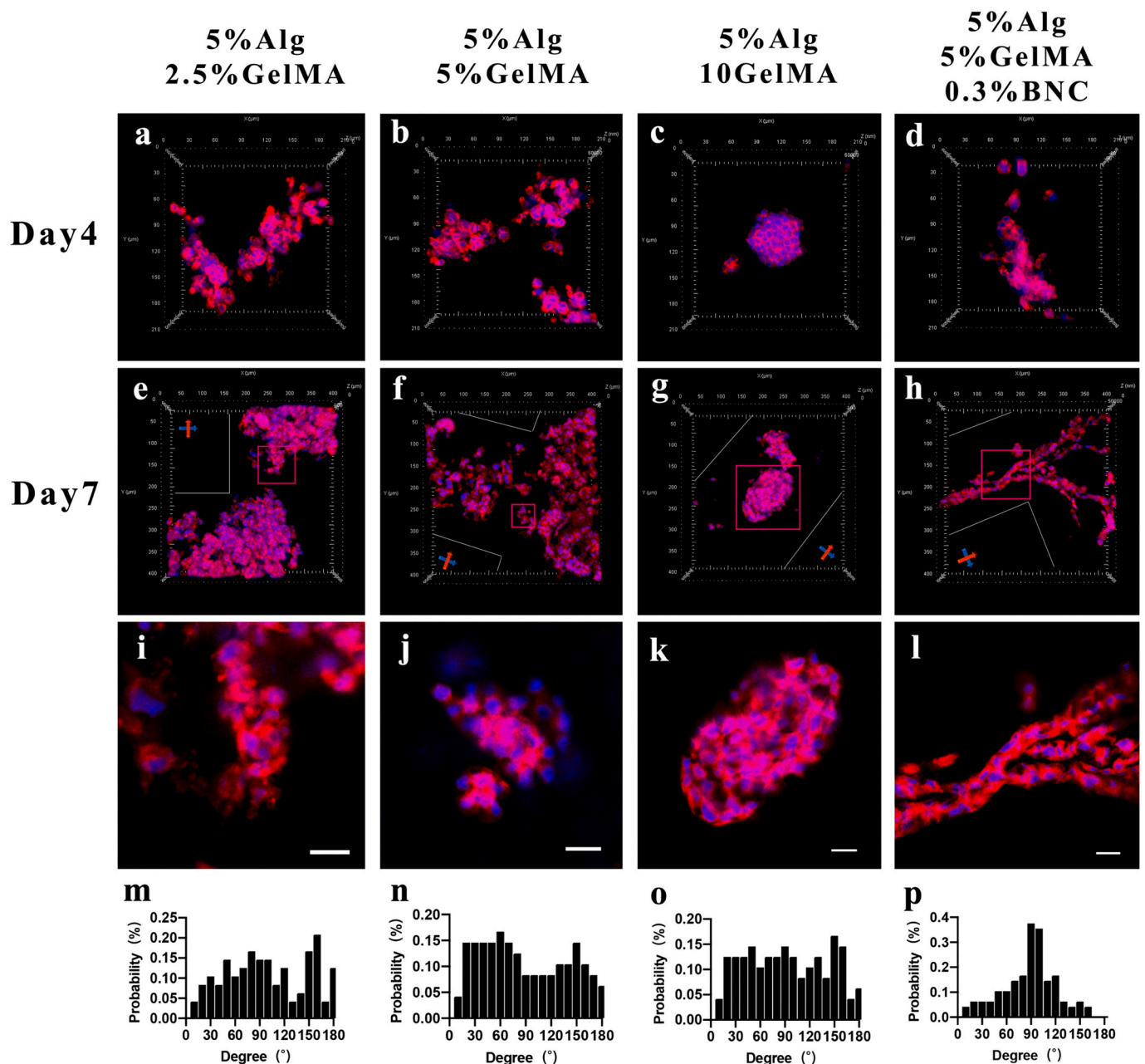


Fig. 8. Cytoskeleton staining on days 4 and 7 of the 2.5% GelMA group (a, e), 5% GelMA group (b, f), 10% GelMA group (c, g), and 5% GelMA+0.3% BNC group (d, h). White line in e,f,g,h shows the outline of the scaffold, and the arrow marks the direction of the long axis of the scaffold. (i, j, k, l) is to enlarge the area of each group of red boxes in (e, f, g, h). The angle between the long axis of the cell and the vertical line to the long axis of the scaffold was calculated and the percentage of (m) 2.5% GelMA group, (n) 5% GelMA group, (o) 10% GelMA group, (p) 5% GelMA+0.3% BNC group was counted. (For interpretation of the references to colour in this figure legend, the reader is referred to the web version of this article.)

3.4. Analysis of S-100 β staining and cytoskeleton staining

S100 β is a typical cytoplasmic marker protein of Schwann cells that is related to the proliferation of nerve cells and the expression of functional proteins. S100 β can also be stably expressed in RSC96 cells. Li et al. [50] used gelatin-alginate scaffolds mixed with RSC96 cells in 3D-bioprinted nerve scaffolds. After 7 days, RSC96 cells stably expressed S-100 β . On day 4 after printing, an S100 β antibody was used to directly stain the printed forms in each group. According to Fig. 7, most of the cells expressed S100 β , which indicated that the 3D bioprinting process and 3D culture did not inhibit S100 β expression. In addition, in the 5% GelMA+0.3% BNC group, the cells formed an obviously oriented arrangement, as shown in Fig. 7d, which was consistent with the live/

dead staining results. However, the cells in the 2.5% GelMA group, 5% GelMA group and 10% GelMA group grew in clusters, and the cells did not form obviously oriented junctions. It has been proven that human breast cancer cells cultured on 3D-printed collagen structures can be aligned along the direction of a collagen fibre arrangement [51]. Zhang et al. [52] produced micropatterned polycaprolactone (PCL) scaffolds and cultured Schwann cells on them. The results showed that they could help Schwann cells release nerve growth factor (NGF), brain-derived neurotrophic factor (BDNF) and other growth factors. The oriented growth of Schwann cells is helpful to form axonal structures, which are more conducive to peripheral nerve regeneration than cluster growth [53]. Similar results can be found in Fig. 8 cytoskeleton staining. In the 5% GelMA+0.3% BNC group of day7, the cells grew in spindle shape and

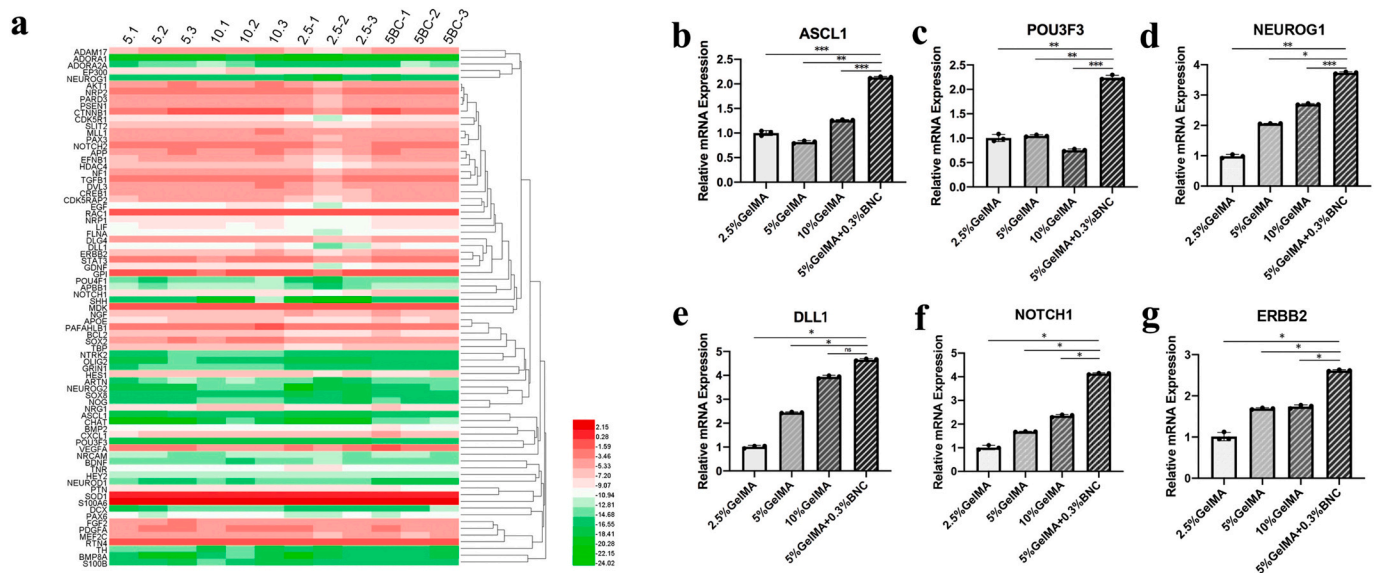


Fig. 9. a) PCR array heatmap of 92 genes. b-g) Quantitative comparison of ASCL1, POU3F3, NEUROG1, DLL1, NOTCH1 and ERBB2 gene expression on day 7 analysed by the $2^{-\Delta\Delta Ct}$ method using GAPDH as the internal control. Dates were represented as the mean \pm SD ($n = 3$). (* $p < 0.05$, ** $p < 0.01$ and *** $p < 0.001$).

formed directional junctions. In the 2.5% GelMA group, 5% GelMA group and 10% GelMA group, the cytoskeletal staining of cells tended to indicate round cell growth, and cell proliferation showed cluster growth from day 4 to day 7, especially in the 10% GelMA group; this growth pattern is not conducive to the biological function of cells. We calculated the angle between the long axis of the cell and the vertical line to the long axis of the scaffold (Fig. 8i-l), and counted the percentage (Fig. 8m-p). The results showed that nearly 72% of the cells in 5% GelMA+0.3% BNC group were parallel or nearly parallel to the long axis of the scaffold, while only 29%, 16% and 26% of the cells in 2.5% GelMA group, 5% GelMA group and 10% GelMA group respectively. The cells in other groups tended to grow disorderly or clumped, while the cells in 5% GelMA+0.3% BNC group grew orderly. Combined with the SEM results, we speculate that by adding BNC, the internal structure of the material formed an orderly layer arrangement. When the materials were fully mixed, the extrusion process of 3D bioprinting can promote the alignment of the internal structure. Moreover, Schwann cells tend to form linear junctions, which is helpful for myelin formation and nerve regeneration [53]. Therefore, RSC96 cells formed an orderly linear

arrangement under the appropriate internal arrangement and shear force.

3.5. PCR array analysis

To elucidate the mechanism of neural regeneration of RSC96 cells in each group of biomaterials, we used a PCR array to detect 92 genes related to neural regeneration in each group on day 7. The results (Fig. 9) showed that the expression levels of ASCL1, POU3F3, NEUROG1, DLL1, NOTCH1 and ERBB2 in the 5% GelMA+0.3% BNC group were higher than those in the other groups. ASCL1 is a basic regulator of axon growth, which is closely related to the establishment of the peripheral nerve ganglion [54], and can promote functional recovery after nerve injury by regulating the expression of DLL1 [55]. At the same time, high expression of POU3F3 [56] and NEUROG1 can induce the expression of neural factors-DLL1 [57], which was similar to the results of this experiment. DLL1 belongs to delta/serrate/Jagged family. It interacts with Notch receptors and regulates Schwann cell proliferation and functional expression through signal transduction [58]. NRG1-

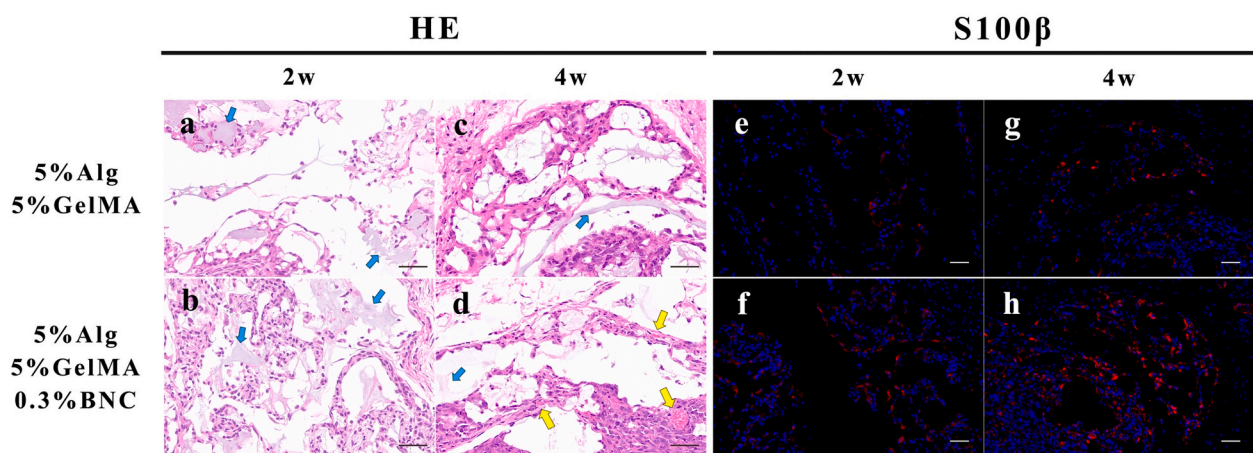


Fig. 10. In vivo experiment: HE staining of paraffin embedded sections at 2 and 4 weeks after implantation in the 5% GelMA group (a,c) and 5% GelMA+0.3% BNC group(b, d), the scale bar is 50 μ m (blue arrows indicate scaffold residue, yellow arrows indicate blood vessels). S100 β immunohistochemical staining at 2 and 4 weeks in the 5% GelMA group (e, f) and 5% GelMA+0.3% BNC group (g, h); red for S100 β , blue for DAPI, and the scale bar is 50 μ m. (For interpretation of the references to colour in this figure legend, the reader is referred to the web version of this article.)

ERBB2 signal controls the survival, proliferation, migration, maturation and myelination of Schwann cells [59]. We speculated that because the RSC96 cells tended to adhere and extend on the surface of materials with higher modulus [60], and the appropriate porosity help to enhance the adhesion and mobility of Schwann cells on the matrix [61]. ASCL1, POU3F3 and NEUROG1 can activate the Notch ligand DLL1 when RSC96 cells adhere better and connect regularly [62]. Furthermore, it can activate Notch 1 receptor on Schwann cells and enhance NRG1-ERBB2 signal transduction, which contributes to Schwann cell proliferation, functional expression and myelination [59].

3.6. *In vivo* experiments

3D-printed scaffolds with cells were implanted in nude mice for 2 and 4 weeks and then harvested for HE staining and S-100 β staining (S. Fig. 2). At the second week, HE staining (Fig. 10a,b) showed that the 5% GelMA group had a loose reticular structure. Concurrently, the 5% GelMA+0.3% BNC group had a more compact structure, which may be related to the supportive effect of BNC on the scaffold. A certain amount of scaffold residues was observed in both groups. At the same time, both groups of structural cells were S-100 β positive (Fig. 10e, f). At the fourth week, the scaffold volume of the 5% GelMA+0.3% BNC group was larger than that of the 5% GelMA group, which may be due to the microenvironment of cells, which is more conducive to proliferation and expression. Local blood vessels grew into the scaffold (Fig. 10d), and the positive area of S100 β was larger (Fig. 10g-h). Meanwhile, the scaffold residues in the two groups were less, indicating that the scaffold material had undergone a certain degree of degradation. Some studies used 3D-bioprinted gelatine-alginate scaffolds and implanted them in nude mice for 8 weeks. The results showed that the scaffold containing cells maintained the original shape and that the blood vessels grew into the structure [63]. Luo et al. [64] used 3D-bioprinted 5% GelMA scaffolds loaded with bone marrow MSCs (BMSCs). The results showed that 21 days later, the nude mice showed suitable growth without systemic or local inflammation and toxicity, and local cartilage fossa had formed. Combined with the results of this study, it has been proven that a 3D-printed structure is helpful for the growth of RSC96 cells.

Sodium alginate can be mixed with carbon nanotubes, methyl cellulose and poly lysine for 3D printing. Poly lysine can promote cell connection and cell aggregation, so as to help cells better play their functions, but its mechanical properties basically depend on the cross-linking of sodium alginate and calcium ions [65]. Carbon nanotubes and methyl cellulose can increase the mechanical strength of the material, but the doping amount of carbon nanotubes should not exceed 1%, otherwise it will produce greater cytotoxicity [66]. The addition of 9 wt% methyl cellulose significantly improved the cyclic compression and thixotropy of the composites [67]. However, due to the lack of cellulase in human body, high content of cellulose should concern the problem of degradation *in vivo*. In this study, we used alginate-GelMA to construct the main components of the scaffold, which provided a good living environment for RSC96 cells. 0.3%BNC enhanced the mechanical strength of the scaffolds and promoted the growth of RSC96 cells. In the future research, we will focus on using 3D bioprinting to improve the internal design of the scaffold, so as to achieve better growth of nerve cells in the scaffold and even nerve regeneration.

4. Conclusion

In this study, 3D bioprinting was successfully applied to construct a hydrogel structure composed of alginate, GelMA and BNC; its physicochemical properties were better than those of other control groups. At the same time, it was confirmed that the 3D-bioprinted construct could promote oriented growth, proliferation and adhesion of RSC96 cells and promote the expression of ASCL1, POU3F3, NEUROG1, DLL1, NOTCH1 and ERBB2 genes. These preliminary results indicated that 3D bioprinting of sodium alginate, GelMA and BNC constructs provides a

suitable microenvironment for RSC96 cells to maintain their activity and biological function. Therefore, 3D-bioprinted sodium alginate, GelMA and BNC constructs are expected to become candidate materials for neural tissue engineering.

CRediT authorship contribution statement

Zongxi Wu: Conceptualization, Methodology, Formal analysis, Investigation, Writing – original draft. **Shang Xie:** Project administration, Writing – review & editing. **Yifan Kang:** Visualization, Writing – review & editing, Funding acquisition. **Xiaofeng Shan:** Conceptualization, Writing – review & editing. **Qing Li:** Conceptualization, Supervision, Writing – review & editing, Funding acquisition. **Zhigang Cai:** Conceptualization, Supervision, Funding acquisition.

Declaration of competing interest

The authors declare that they have no known competing financial interests or personal relationships that could have appeared to influence the work reported in this paper.

Acknowledgements

This work was supported by the National Natural Science Foundation of China (No. 81870781), Peking University Hospital of Stomatology Young Foundation (Grant No. PKUSS20200106 & PKUSS20200113).

Appendix A. Supplementary data

Supplementary data to this article can be found online at <https://doi.org/10.1016/j.msec.2021.112393>.

References

- [1] A. Faroni, S.A. Mobasseri, P.J. Kingham, A.J. Reid, Peripheral nerve regeneration: experimental strategies and future perspectives, *Adv. Drug Deliv. Rev.* 82 (83) (2015) 160–167.
- [2] M. Asplund, M. Nilsson, A. Jacobsson, H. von Holst, Incidence of traumatic peripheral nerve injuries and amputations in Sweden between 1998 and 2006, *Neuroepidemiology* 32 (3) (2009) 217–228.
- [3] J. Moskow, B. Ferrigno, N. Mistry, D. Jaiswal, K. Bulsara, S. Rudraiah, S. G. Kumbar, Review: bioengineering approach for the repair and regeneration of peripheral nerve, *Bioact Mater* 4 (1) (2019) 107–113.
- [4] F.J. Paprottka, P. Wolf, Y. Harder, Y. Kern, P.M. Paprottka, H.G. Machens, J. A. Lohmeyer, Sensory recovery outcome after digital nerve repair in relation to different reconstructive techniques: meta-analysis and systematic review, *Plast Surg Int* 2013 (2013), 704589.
- [5] H. Fujimaki, K. Uchida, G. Inoue, M. Miyagi, N. Nemoto, T. Saku, Y. Isobe, K. Inage, O. Matsushita, S. Yagishita, J. Sato, S. Takano, Y. Sakuma, S. Ohtori, K. Takahashi, M. Takaso, Oriented collagen tubes combined with basic fibroblast growth factor promote peripheral nerve regeneration in a 15 mm sciatic nerve defect rat model, *J. Biomed. Mater. Res. A* 105 (1) (2017) 8–14.
- [6] Q. Li, X. Lei, X. Wang, Z. Cai, P. Lyu, G. Zhang, Hydroxyapatite/collagen three-dimensional printed scaffolds and their osteogenic effects on human bone marrow-derived mesenchymal stem cells, *Tissue Eng Part A* 25 (17–18) (2019) 1261–1271.
- [7] J. Yoo, J.H. Park, Y.W. Kwon, J.J. Chung, I.C. Choi, J.J. Nam, H.S. Lee, E.Y. Jeon, K. Lee, S.H. Kim, Y. Jung, J.W. Park, Augmented peripheral nerve regeneration through elastic nerve guidance conduits prepared using a porous PLCL membrane with a 3D printed collagen hydrogel, *Biomater Sci* 8 (22) (2020) 6261–6271.
- [8] K.Y. Lee, D.J. Mooney, Alginate: properties and biomedical applications, *Prog. Polym. Sci.* 37 (1) (2012) 106–126.
- [9] Z. Wu, Q. Li, S. Xie, X. Shan, Z. Cai, *In vitro* and *in vivo* biocompatibility evaluation of a 3D bioprinted gelatin-sodium alginate/rat Schwann-cell scaffold, *Mater. Sci. Eng. C Mater. Biol. Appl.* 109 (2020), 110530.
- [10] T. Liu, W. Weng, Y. Zhang, X. Sun, H. Yang, Applications of gelatin methacryloyl (GelMA) hydrogels in microfluidic technique-assisted tissue engineering, *Molecules* 25 (22) (2020).
- [11] T. Dursun Usal, D. Yucel, V. Hasirci, A novel GelMA-pHEMA hydrogel nerve guide for the treatment of peripheral nerve damages, *Int. J. Biol. Macromol.* 121 (2019) 699–706.
- [12] W. Zhu, K.R. Tringale, S.A. Woller, S. You, S. Johnson, H. Shen, J. Schimelman, M. Whitney, J. Steinauer, W. Xu, T.L. Yaksh, Q.T. Nguyen, S. Chen, Rapid continuous 3D printing of customizable peripheral nerve guidance conduits, *Mater Today (Kidlington)* 21 (9) (2018) 951–959.

- [13] R. Schipani, S. Scheurer, R. Florentin, S.E. Critchley, D.J. Kelly, Reinforcing interpenetrating network hydrogels with 3D printed polymer networks to engineer cartilage mimetic composites, *Biofabrication* 12 (3) (2020), 035011.
- [14] J.M. Rajwade, K.M. Paknikar, J.V. Kumbhar, Applications of bacterial cellulose and its composites in biomedicine, *Appl. Microbiol. Biotechnol.* 99 (6) (2015) 2491–2511.
- [15] S. Samfors, K. Karlsson, J. Sundberg, K. Markstedt, P. Gatenholm, Biofabrication of bacterial nanocellulose scaffolds with complex vascular structure, *Biofabrication* 11 (4) (2019), 045010.
- [16] Y. Fan, Z. Yue, E. Lucarelli, G.G. Wallace, Hybrid printing using cellulose Nanocrystals reinforced GelMA/HAMA hydrogels for improved structural integration, *Adv Healthc Mater* 9 (24) (2020), e2001410.
- [17] S. Ansari, P. Sarrion, M.M. Hasani-Sadrabadi, T. Aghaloo, B.M. Wu, A. Moshaverinia, Regulation of the fate of dental-derived mesenchymal stem cells using engineered alginate-GelMA hydrogels, *J. Biomed. Mater. Res. A* 105 (11) (2017) 2957–2967.
- [18] L. Ouyang, R. Yao, Y. Zhao, W. Sun, Effect of bioink properties on printability and cell viability for 3D bioplotting of embryonic stem cells, *Biofabrication* 8 (3) (2016), 035020.
- [19] L.Y. Daikuara, Z. Yue, D. Skropeta, G.G. Wallace, In vitro characterisation of 3D printed platelet lysate-based bioink for potential application in skin tissue engineering, *Acta Biomater.* 123 (2021) 286–297.
- [20] M. Wang, X. Ge, Y. Zheng, C. Wang, Y. Zhang, Y. Lin, Microarray analysis reveals that lncRNA PWRN1-209 promotes human bone marrow mesenchymal stem cell osteogenic differentiation on microtopography titanium surface in vitro, *J Biomed Mater Res B Appl Biomater* 108 (7) (2020) 2889–2902.
- [21] N. Barros, H. Kim, M.J. Goudie, K. Lee, P. Bandaru, E.A. Banton, E. Sarikhani, W. Sun, S. Zhang, H.J. Cho, M.C. Hartel, S. Ostrovidov, S. Ahadian, S. Hussain, N. Ashammakhi, M.R. Dokmeci, R.D. Herculano, J. Lee, A. Khademhosseini, Biofabrication of endothelial cell, dermal fibroblast, and multilayered keratinocyte layers for skin tissue engineering, *Biofabrication* 13 (3) (2020).
- [22] X. Zhou, M. Nowicki, H. Sun, S.Y. Hann, H. Cui, T. Esworthy, J.D. Lee, M. Plesniak, L.G. Zhang, 3D bioprinting-tunable small-diameter blood vessels with biomimetic biphasic cell layers, *ACS Appl. Mater. Interfaces* 12 (41) (2020) 45904–45915.
- [23] D.F.S. Fonseca, C. Vilela, R.J.B. Pinto, V. Bastos, H. Oliveira, J. Catarino, P. Paisca, C. Rosado, A.J.D. Silvestre, C.S.R. Freire, Bacterial nanocellulose-hyaluronic acid microneedle patches for skin applications: in vitro and in vivo evaluation, *Mater Sci Eng C Mater Biol Appl* 118 (2021), 111350.
- [24] L. Bao, J. Tang, F.F. Hong, X. Lu, L. Chen, Physicochemical properties and in vitro biocompatibility of three bacterial Nanocellulose conduits for blood vessel applications, *Carbohydr. Polym.* 239 (2020), 116246.
- [25] H. Li, Y.J. Tan, R. Kiran, S.B. Tor, K. Zhou, Submerged and non-submerged 3D bioprinting approaches for the fabrication of complex structures with the hydrogel pair GelMA and alginate/methylcellulose, *Additive Manufacturing* (2021) 37.
- [26] L. Gu, T. Li, X. Song, X. Yang, S. Li, L. Chen, P. Liu, X. Gong, C. Chen, L. Sun, Preparation and characterization of methacrylated gelatin/bacterial cellulose composite hydrogels for cartilage tissue engineering, *Regen Biomater* 7 (2) (2020) 195–202.
- [27] S. Lopes, L. Bueno, F.J. Aguiar, C. Finkler, Preparation and characterization of alginate and gelatin microcapsules containing lactobacillus rhamnosus, *An. Acad. Bras. Cienc.* 89 (3) (2017) 1601–1613.
- [28] W. Weng, W. Wu, X. Yu, M. Sun, Z. Lin, M. Ibrahim, H. Yang, Effect of GelMA hydrogel coatings on corrosion resistance and biocompatibility of MAO-coated mg alloys, *Materials (Basel)* 13 (17) (2020).
- [29] K.M. Dokken, L.C. Davis, N.S. Marinkovic, Use of infrared microspectroscopy in plant growth and development, *Appl. Spectrosc. Rev.* 40 (4) (2005) 301–326.
- [30] G. Chen, L. Chen, W. Wang, F.F. Hong, M. Zhu, Manufacture of a novel anisotropic bacterial nanocellulose hydrogel membrane by using a rotary drum bioreactor, *Carbohydr. Polym.* 211 (2019) 281–288.
- [31] A. Abraham, V.R. Jothi, J. Lee, S.-C. Yi, B.-J. Sang, Bacterial nanocellulose as a green and flexible electrode matrix for efficient hydrogen evolution reaction in alkaline conditions, *Cellulose* 27 (14) (2020) 8135–8146.
- [32] S. Dutta, J. Kim, Y. Ide, J. Ho Kim, M.S.A. Hossain, Y. Bando, Y. Yamauchi, K.C. W. Wu, 3D network of cellulose-based energy storage devices and related emerging applications, *Materials Horizons* 4 (4) (2017) 522–545.
- [33] Y. Sun, Q. Quan, H. Meng, Y. Zheng, J. Peng, Y. Hu, Z. Feng, X. Sang, K. Qiao, W. He, X. Chi, L. Zhao, Enhanced neurite outgrowth on a multiblock conductive nerve scaffold with self-powered electrical stimulation, *Adv Healthc Mater* 8 (10) (2019), e1900127.
- [34] T. Gordon, A.W. English, Strategies to promote peripheral nerve regeneration: electrical stimulation and/or exercise, *Eur. J. Neurosci.* 43 (3) (2016) 336–350.
- [35] J. Yin, M. Yan, Y. Wang, J. Fu, H. Suo, 3D bioprinting of low-concentration cell-laden gelatin methacrylate (GelMA) bioinks with a two-step cross-linking strategy, *ACS Appl. Mater. Interfaces* 10 (8) (2018) 6849–6857.
- [36] P.R. Chawla, I.B. Bajaj, S.A. Survase, R.S. Singha, Microbial cellulose: fermentative production and applications, *Food Technol. Biotechnol.* 47 (2) (2009) 107–124.
- [37] N. Soykeabkaew, C. Sian, S. Gea, T. Nishino, T. Peijs, All-cellulose nanocomposites by surface selective dissolution of bacterial cellulose, *Cellulose* 16 (3) (2009) 435–444.
- [38] P.M. Favi, S.P. Ospina, M. Kachole, M. Gao, L. Atehortua, T.J. Webster, Preparation and characterization of biodegradable nano hydroxyapatite–bacterial cellulose composites with well-defined honeycomb pore arrays for bone tissue engineering applications, *Cellulose* 23 (2) (2016) 1263–1282.
- [39] I. Pepelanova, K. Kruppa, T. Scheper, A. Lavrentieva, Gelatin-methacryloyl (GelMA) hydrogels with defined degree of functionalization as a versatile toolkit for 3D cell culture and extrusion bioprinting, *Bioengineering (Basel)* 5 (3) (2018).
- [40] G.H. Yang, W. Kim, J. Kim, G. Kim, A skeleton muscle model using GelMA-based cell-aligned bioink processed with an electric-field assisted 3D/4D bioprinting, *Theranostics* 11 (1) (2021) 48–63.
- [41] K. Yue, G. Trujillo-de Santiago, M.M. Alvarez, A. Tamayol, N. Annabi, A. Khademhosseini, Synthesis, properties, and biomedical applications of gelatin methacryloyl (GelMA) hydrogels, *Biomaterials* 73 (2015) 254–271.
- [42] W. Xu, B.Z. Molino, F. Cheng, P.J. Molino, Z. Yue, D. Su, X. Wang, S. Willfor, C. Xu, G.G. Wallace, On low-concentration inks formulated by nanocellulose assisted with gelatin methacrylate (GelMA) for 3D printing toward wound healing application, *ACS Appl. Mater. Interfaces* 11 (9) (2019) 8838–8848.
- [43] M.M. Pillai, H.N. Tran, G. Sathishkumar, K. Manimekalai, J. Yoon, D. Lim, I. Noh, A. Bhattacharyya, Symbiotic culture of nanocellulose pellicle: a potential matrix for 3D bioprinting, *Mater. Sci. Eng. C Mater. Biol. Appl.* 119 (2021), 111552.
- [44] A. Cañas-Gutiérrez, E. Martínez-Correa, D. Suárez-Avenida, D. Arboleda-Toro, C. Castro-Herazo, Influence of bacterial nanocellulose surface modification on calcium phosphates precipitation for bone tissue engineering, *Cellulose* 27 (18) (2020) 10747–10763.
- [45] C. Sharma, N.K. Bhardwaj, P. Pathak, Ternary nano-biocomposite films using synergistic combination of bacterial cellulose with chitosan and gelatin for tissue engineering applications, *J. Biomater. Sci. Polym. Ed.* (2020) 1–23.
- [46] E.H. Barriga, E. Theveneau, In vivo neural crest cell migration is controlled by “Mixotaxis”, *Front. Physiol.* 11 (2020), 586432.
- [47] Y. Wu, A. Wenger, H. Golzar, X.S. Tang, 3D bioprinting of bicellular liver lobule-mimetic structures via microextrusion of cellulose nanocrystal-incorporated shear-thinning bioink, *Sci. Rep.* 10 (1) (2020) 20648.
- [48] P. Apelgren, E. Karabulut, M. Amoroso, A. Mantas, H. Martinez Avila, L. Kolby, T. Kondo, G. Toriz, P. Gatenholm, In vivo human cartilage formation in three-dimensional bioprinted constructs with a novel bacterial nanocellulose bioink, *ACS Biomater Sci Eng* 5 (5) (2019) 2482–2490.
- [49] M. Osorio, P. Fernandez-Morales, P. Ganan, R. Zuluaga, H. Kerguelen, I. Ortiz, C. Castro, Development of novel three-dimensional scaffolds based on bacterial nanocellulose for tissue engineering and regenerative medicine: effect of processing methods, pore size, and surface area, *J. Biomed. Mater. Res. A* 107 (2) (2019) 348–359.
- [50] X. Li, X. Wang, X. Wang, H. Chen, X. Zhang, L. Zhou, T. Xu, 3D bioprinted rat Schwann cell-laden structures with shape flexibility and enhanced nerve growth factor expression, *3 Biotech* 8 (8) (2018) 342.
- [51] B.A. Neger, P.T. Brun, C.M. Nelson, Microextrusion printing cell-laden networks of type I collagen with patterned fiber alignment and geometry, *Soft Matter* 15 (28) (2019) 5728–5738.
- [52] L. Zhang, S. Chen, R. Liang, Y. Chen, S. Li, S. Li, Z. Sun, Y. Wang, G. Li, A. Ming, Y. Yang, Fabrication of alignment polycaprolactone scaffolds by combining use of electrospinning and micromolding for regulating Schwann cells behavior, *J. Biomed. Mater. Res. A* 106 (12) (2018) 3123–3134.
- [53] S. Chen, C. Wu, A. Liu, D. Wei, Y. Xiao, Z. Guo, L. Chen, Y. Zhu, J. Sun, H. Luo, H. Fan, Biofabrication of nerve fibers with mimetic myelin sheath-like structure and aligned fibrous niche, *Biofabrication* 12 (3) (2020), 035013.
- [54] V. Dyachuk, A. Furlan, M.K. Shahidi, M. Giovenco, N. Kauka, C. Konstantinidou, V. Pachnis, F. Memic, U. Marklund, T. Müller, C. Birchmeier, K. Fried, P. Ernfors, I. Adameyko, Neurodevelopment parasymphathetic neurons originate from nerve-associated peripheral glial progenitors, *Science* 345 (6192) (2014) 82–87.
- [55] R.R. Williams, I. Venkatesh, D.D. Pearce, A.J. Udvadia, M.B. Bunge, MASH1/Ascl1a leads to GAP43 expression and axon regeneration in the adult CNS, *PLoS One* 10 (3) (2015), e0118918.
- [56] K. Nakayama, K. Nagase, Y. Tokutake, C.S. Koh, M. Hiratochi, T. Ohkawara, N. Nakayama, Multiple POU-binding motifs, recognized by tissue-specific nuclear factors, are important for Dll1 gene expression in neural stem cells, *Biochem. Biophys. Res. Commun.* 325 (3) (2004) 991–996.
- [57] S. Han, D.J. Dennis, A. Balakrishnan, R. Dixit, O. Britz, D. Zinyk, Y. Touahri, T. Olender, M. Brand, F. Guillemot, D. Kurrasch, C. Schuurmans, A non-canonical role for the proneural gene Neurog1 as a negative regulator of neocortical neurogenesis, *Development* 145 (19) (2018).
- [58] A. Murata, K. Okuyama, S. Sakano, M. Kajiki, T. Hirata, H. Yagita, J.C. Zuniga-Pflucker, K. Miyake, S. Akashi-Takamura, S. Moriawaki, S. Niida, M. Yoshino, S. Hayashi, A Notch ligand, Delta-like 1 functions as an adhesion molecule for mast cells, *J. Immunol.* 185 (7) (2010) 3905–3912.
- [59] K.R. Jessen, R. Mirsky, Schwann cell precursors; multipotent glial cells in embryonic nerves, *Front. Mol. Neurosci.* 12 (2019) 69.
- [60] S. Bell, A.L. Redmann, E.M. Terentjev, Universal kinetics of the onset of cell spreading on substrates of different stiffness, *Biophys. J.* 116 (3) (2019) 551–559.
- [61] S. Shahidi, M. Janmaleki, S. Riaz, A. Sanati Nezhad, N. Syed, A tuned gelatin methacryloyl (GelMA) hydrogel facilitates myelination of dorsal root ganglia neurons in vitro, *Mater. Sci. Eng. C Mater. Biol. Appl.* 126 (2021), 112131.
- [62] E.R. Wilson, G. Della-Flora Nunes, M.R. Weaver, L.R. Frick, M.L. Feltri, Schwann cell interactions during the development of the peripheral nervous system, *Dev Neurobiol* 81 (5) (2021) 464–489.
- [63] X.F. Wang, Y. Song, Y.S. Liu, Y.C. Sun, Y.G. Wang, Y. Wang, P.J. Lyu, Osteogenic differentiation of three-dimensional bioprinted constructs consisting of human adipose-derived stem cells in vitro and in vivo, *PLoS One* 11 (6) (2016), e0157214.
- [64] C. Luo, R. Xie, J. Zhang, Y. Liu, Z. Li, Y. Zhang, X. Zhang, T. Yuan, Y. Chen, W. Fan, Low-temperature three-dimensional printing of tissue cartilage engineered with gelatin methacrylamide, *Tissue Eng Part C Methods* 26 (6) (2020) 306–316.
- [65] S. Saberianpour, A. Rezaie Nezhad Zamani, A. Karimi, M. Ahmadi, N. Khatami, A. Pouyafar, R. Rahbarghazi, M. Nouri, Hollow alginate-poly-L-lysine-alginate

- microspheres promoted an epithelial-Mesenchymal transition in human colon adenocarcinoma cells, *Adv Pharm Bull* 10 (1) (2020) 141–145.
- [66] L. Li, S. Qin, J. Peng, A. Chen, Y. Nie, T. Liu, K. Song, Engineering gelatin-based alginate/carbon nanotubes blend bioink for direct 3D printing of vessel constructs, *Int. J. Biol. Macromol.* 145 (2020) 262–271.
- [67] H. Li, Y.J. Tan, K.F. Leong, L. Li, 3D bioprinting of highly thixotropic alginate/methylcellulose hydrogel with strong Interface bonding, *ACS Appl. Mater. Interfaces* 9 (23) (2017) 20086–20097.